Published in final edited form as:
Biomaterials. 2008 December ; 29(35): 4650–4657. doi:10.1016/j.biomaterials.2008.08.025.

Gel spinning of silk tubes for tissue engineering

Michael Lovett[a], **Christopher Cannizzaro**[a], **Gordana Vunjak-Novakovic**[b], and **David L. Kaplan**[a,*]

[a] Department of Biomedical Engineering, Tufts University, 4 Colby St., Medford, Massachusetts 02155, USA

[b] Department of Biomedical Engineering, Columbia University, 351 Engineering Terrace, 1210 Amsterdam Ave., MC 8904, New York, New York 10027, USA

Abstract

Tubular vessels for tissue engineering are typically fabricated using a molding, dipping, or electrospinning technique. While these techniques provide some control over inner and outer diameters of the tube, they lack the ability to align the polymers or fibers of interest throughout the tube. This is an important aspect of biomaterial composite structure and function for mechanical and biological impact of tissue outcomes. We present a novel aqueous process system to spin tubes from biopolymers and proteins such as silk fibroin. Using silk as an example, this method of winding an aqueous solution around a reciprocating rotating mandrel offers substantial improvement in the control of the tube properties, specifically with regard to winding pattern, tube porosity, and composite features. Silk tube properties are further controlled via different post-spinning processing mechanisms such as methanol-treatment, air-drying, and lyophilization. This approach to tubular scaffold manufacture offers numerous tissue engineering applications such as complex composite biomaterial matrices, blood vessel grafts and nerve guides, among others.

Keywords

Silk; vascular grafts; arterial tissue engineering; mechanical properties; endothelial cells; smooth muscle cells

1. Introduction

The demand for tubular constructs for tissue engineering is high given the interest in microvascular grafts[1-3], nerve guides[4], and pre-vascularized tissues[5, 6]. In order to form vessels with desired properties for a given application, a system is required that can functionally control parameters and processing methods to reproducibly manufacture tubes with relevant properties. To date, vessels have been commonly made using biodegradable scaffolds[7, 8] and tubular molds[9], methods where the scaffold deposition is accomplished without control of polymer or fiber alignment, or by electrospinning[10], which requires optimization of several processing steps (e.g., mandrel selection, voltage, and humidity). Thus, it remains an open challenge to generate tubular constructs with control over the

* Corresponding author. Tel.: +1-617-627-3251; fax: +1-617-627-3231. David.Kaplan@tufts.edu (D.L. Kaplan)..

material deposition, and hence control over the resultant mechanical and biological properties of the vessel. The importance of aligned protein polymers and fibers in extracellular matrix structure permeates almost all tissue structures and provides an architectural basis for tissue function[11-13]. Thus, an ability to recapitulate aspects of this structural organization in biomaterial composites would provide an important step forward in scaffold designs to mimic native tissue features.

We address this challenge by using a natural biopolymer, silk fibroin, which offers unique and robust mechanical properties along with versatile processing options to permit the formation of tubular systems. To accomplish this goal, tubes were wound using a reciprocating rotating mandrel. This approach provides excellent control over tube properties through appropriate selection of silk processing, winding strategy, and post-winding processing.

Previously we reported the development of silk microtubes for blood vessel repair with several advantages over existing scaffold materials/designs[3]. These advantages were based upon the unique properties of silk fibroin[14], specifically its mechanical strength and toughness, as well as the ease of tube production using a simple dipping technique. In addition, as a protein, silk can be chemically modified with functional groups to serve specific functions. The simplicity of the dipping technique, however, does not allow for fine control over tube wall thickness, uniformity and pore size/distribution [3]. We have since refined this method whereby silk properties and resultant tube properties are substantially improved by winding an aqueous silk solution around a reciprocating rotating mandrel. Gel spinning processes have been previously used to form uniform tubes or fibers from polymers such as poly(L-lactide-co-caprolactone) (PLCL)[15], chitosan[16], and gelatin[17], among others. These polymers, however, are typically spun using non-aqueous solvents and do not demonstrate the same level of control over fiber alignment and orientation as achieved here. Driving the silk through a small gauge needle induces a shear stress upon the amorphous concentrated fibroin (silk I), which helps to exclude water from the protein solution, align the silk fibrils, and induce silk II (antiparallel β-sheet, aqueous insoluble) structure[18, 19]. This process mimics the process of protein spinning in the native silkworm, where fibroin concentration and physical shear play critical roles in the spinneret[20]. The gel spinning process allows properties such as winding pattern, pore size, and tube composition to be controlled in the new process described here, with further options during post-winding processing via treatment with methanol, air-drying, and/or lyophilization. Silk fibroin tubes generated using this new process have applications within tissue engineering, from blood vessel grafts and nerve guidance channels to *in vitro* migration assays, permeability studies, and novel composite scaffolds in general.

2. Materials and methods

2.1. Winding device

A custom silk spinning device was designed in standard CAD program (Solidworks, Concord, MA), with resultant parts machined from aluminum, Delrin, and Teflon. The silk spinning mandrel was driven by a two axis stepper motor (Haydon Switch & Instrument, Waterbury, CT) that drove the mandrel both axially and rotationally. The motor was driven through the use of a stepper motor controller board (Peter Norberg Consulting, Ferguson, MO) and controlled through a custom program written in LabVIEW (National Instruments, Austin, TX). Rotational speeds varied from 0-200 rpm while axial speed ranged from 0-40 mm/s over the maximum 2” (5 cm) stroke length. Teflon-coated stainless steel rod (1 mm diameter, McMaster-Carr, Atlanta, GA) was used as the silk spinning mandrel, and was fixed to the motor shaft with a coupling adapter. The rod was stabilized by Teflon guide blocks, allowing the ends of the rod to slide freely. The rod was housed within ¼” (6.35

mm) tubing to allow for nitrogen gas drying of the tube, which was coupled to the Teflon guide block assembly. For silk material deposition, a three-axis manipulator was used to precisely position the syringe needle. Gross manipulation was performed by rotating a custom syringe holder and sliding blocks to pass the needle through a precise hole in the tubing surrounding the mandrel. A second three-axis manipulator and syringe were used for the deposition of a second silk composition or methanol.

2.2. Preparation of aqueous silk fibroin solutions

A 6-8% (w/v) silk fibroin aqueous solution was obtained from *Bombyx mori* silkworm cocoons using previously described procedures[21, 22]. Briefly, the silkworm cocoons (supplied by Tajima Shoji Co., LTD., Yokohama, Japan) were extracted in 0.02 M sodium carbonate solution, rinsed in distilled water, dissolved in 9.3 M lithium bromide, and dialyzed against distilled water using a Slide-a-Lyzer dialysis cassette (molecular weight cutoff MWCO, 3,500, Pierce, Rockford, IL) for 48 hours. The resulting 6-8% (w/v) fibroin solution was then concentrated by dialyzing against 10 wt% poly(ethylene glycol) (PEG) to produce a 20-30% (w/v) silk fibroin aqueous solution. All silk fibroin solutions were stored at 4ºC until used to make silk tubes.

2.3 Winding of silk tubes

Tubes were prepared by pushing 20-30% (w/v) silk fibroin solution through a 27 or 30 gauge needle onto rotating and axially reciprocating mandrel. After evenly coating with concentrated silk fibroin, transformation from amorphous liquid to the β-form silk fibroin conformation characterized by anti-parallel β-sheets was induced by treatment with methanol and/or drying under nitrogen gas[23]. Porous silk tubes were generated with different winding patterns and different numbers of layers, creating tubes of altered pore size and distribution. Additional complexity in the silk tubes was introduced by winding two or three different solutions in the same tubular construct. This was demonstrated by mixing fluorescent latex beads (10 μm diameter, Invitrogen, Carlsbad, CA) or fluorescence-conjugated dextran or bovine serum albumin (50 μg/mL in silk, Invitrogen, Carlsbad, CA) with the silk solutions and winding them as given above and imaged using fluorescent microscopy. Under any tube formation technique, the silk-coated mandrel was placed in a surfactant solution to remove the silk tube from the Teflon-coated stainless steel rod.

2.4. Imaging of silk tubes – SEM and fluorescent microscopy

Scanning electron microscopy (SEM) was used to assess the winding patterns of the silk tubes as well as to confirm the different pore size distributions generated using the specific winding techniques. Tube samples were sputter coated with gold using a Polaron SC502 Sputter Coater (Fisons, VG Microtech, East Sussex, England) and imaged using a JEOL JSM-840 Scanning Microscope (JEOL Ltd., Tokyo, Japan). The SEM images, along with image analysis software (ImageJ, National Institutes of Health, USA) were used to determine the wound fiber widths and pore distribution of the silk tubes. Fluorescence images of the silk tubes were acquired using either an Axiovert 200 fluorescent microscope (Zeiss, Thornwood, NY) or a Leica DMIRE2 confocal microscope with a TCS SP2 scanner (Leica Microsystems, Mannheim/Wetzlar, Germany).

2.5 Mechanical evaluation of silk tubes

Tensile tests were performed on hydrated silk tubes using an Instron 3366 testing frame with a 10N capacity load cell and Biopuls pneumatic clamps. Sample tubes (N=3-4 for each tube type) were hydrated in 0.1M phosphate buffered saline (PBS) for approximately 30 minutes before clamping and submerging in a temperature-controlled Biopuls bath (37 ± 0.3 °C) filled with PBS for at least 5 minutes prior to testing. The initial length of each tube was

obtained using a caliper, and the cross-sectional area estimated using confocal images of previous tubes and the microscope software. A crosshead displacement rate of 5 mm/min was used, with tensile stress and strain graphed on a chart. The linear elastic modulus was calculated using a least-squares fitting between 0.1N load and 2.5% strain past that point. The yield strength was determined by offsetting this least-squares line by 2% strain and marking the data intercept. Ultimate tensile strength was the highest stress value attained during the test and the elongation to failure was the last data point before a >10% decrease in the load.

2.6. Cell culture in silk tubes

Human coronary artery smooth muscle cells (HCASMCs) and a GFP-expressing line of human umbilical vein endothelial cells (GFP-HUVECs) were used to seed the silk tubes[3, 24]. Prior to seeding, they were cultured according to previously reported protocols where GFP-HUVECs were grown in optimized growth media EGM-2 (Lonza, Walkersville, MD) supplemented with 100 U/mL penicillin, 1000 U/mL streptomycin, and 0.2% fungizone antimycotic (GIBCO, Carlsbad, CA), and HCASMCs were cultured in smooth muscle cell medium (SMCM) with 2% fetal bovine serum (FBS), 1% smooth muscle cell growth supplement, and 1% penicillin/streptomycin solution (ScienCell Research Laboratories, Carlsbad, CA). Prior to cell seeding, HCASMCs were stained using a red CellTracker dye at a concentration of 10 μM according to company protocols (Invitrogen, Carlsbad, CA).

Silk tubes were seeded using a previously described bioreactor system[3]. Silk tubes were hydrated and sterilized using distilled water and ethanol, respectively, before inserting into the bioreactor, spanning two 19 gauge needles with media added to pre-condition the tubes. Red HCASMCs were injected into the tube at a concentration of 5×10^6 cells/mL using a syringe and cultured for 3-4 days before adding GFP-HUVECs. GFP-HUVECs were injected into the silk tube in the same manner as the HCASMCs, at a concentration of 5×10^6 cells/mL, and cultured for an additional day before imaging using confocal microscopy.

3. Results and discussion

3.1. Silk spinning – design and winding process

To form tailored silk tubes, a liquid silk spinning device was custom-designed and built, allowing deposition of silk onto a reciprocating rotating mandrel. This device allowed for unlimited control of winding parameters based not only on the range of rotational and axial speeds, but also through the use of offsets built into the program that could shift position of the silk with each successive stroke of the mandrel. This provided control of pore size and specific winding patterns, generating custom silk tubes based on the varied processing parameters. The key to defining the processing parameters was the design of a flowchart system characterizing each tube type (Fig. 1a). Processing parameters were defined at three different levels, silk processing, liquid silk spinning, and post-winding processing. In the silk processing step, as described in previous studies, regenerated silk fibroin may be solubilized using an organic solvent (e.g., hexafluoro-2-propanol (HFIP))[25] or via an all aqueous process[26]. In this study we concentrated solely on the all aqueous-based processing method, paying particular attention to the concentration and viscosity of the aqueous silk solution. Gel spinning was subject to failure at low silk concentrations due to inadequate shear for aligning silk fibrils, and at high concentrations due to pre-gelation in the syringe[27].

The winding angle for liquid silk spinning was adjusted by varying the axial slew rate, while maintaining constant rotational speed. The winding angle, θ, was defined as the angle of the spun silk to the horizontal plane of the mandrel and is given by the equation $\theta = \tan^{-1}(2\pi RV_{ROT}/V_{AXIAL})$, where R is the radius of the mandrel (1 mm for all experiments in

this work), V_{ROT} is the revolutions per minute of the mandrel (200 RPM for all experiments), and V_{AXIAL} is the linear velocity of the motor (mm/min). Four examples of winding parameters were selected to demonstrate this precise control, ranging from a simple wrapping (A, V_{AXIAL} = 2 mm/s) to more complex crisscross designs (B (10 mm/s), C (20 mm/s), and D (40 mm/s)) (Fig. 3). Based on these spinning parameters, silk winding fibers were typically 404 ± 31 μm in width for the wrapping wind (A, 2 mm/s) and 177 ± 74 μm in width for the crisscross winding patterns (B, C, and D) (Fig. 1b, 2). This discrepancy in fiber spinning width relates back to the shear force applied to the silk by the needle in conjunction with the extrusion effect of the rotating and reciprocating mandrel. In the case of the crisscrossing patterns, the movement of the mandrel acts to draw out the silk, pulling and stretching the silk as it is sheared out of the needle. This force acts to thin out the fibers in a way not seen in the wrapping wind, which has a negligible axial component, resulting in less fiber pulling and wider fiber diameters.

3.2. Silk spinning – post-winding processing

Post-winding processing options included methanol treatment, air-drying, and lyophilization, which were defined as 1, 2, and 3, respectively, in the processing flowchart. This combination of winding patterns and post-winding processing techniques allows for 12 different settings (Fig. 1b), while also providing a straightforward nomenclature system for describing each tube type, e.g. a 2 mm/s wound tube treated with methanol is defined as an A1 tube while a tube made using an axial velocity of 20 mm/s and lyophilized is defined as a C3 tube. Each different winding or post-winding processing step provides a unique measure of control over the resultant tube properties, allowing for composite tubes with different windings and post-winding processing techniques in one tube for more advanced applications.

Tube treatment with methanol treatment, air-drying, and/or lyophilization had a significant impact on the final tube results (Fig. 3). In post-winding processing, tubes that were subjected to methanol treatment were immediately induced into β-sheet formation, providing stability in the aqueous solution[28]. This conserved the outer morphology of the winding patterns as they were well defined throughout the length of the tube (Fig. 2, 3). However, this treatment also induced a stratified structure within the tube as observed in tube cross-sections (Fig. 3). Small gaps are clearly visible between each methanol-treated layer. By using an air-drying technique, winding pattern morphology is less pronounced than with the methanol treatment, a primary result of the layering of the silk tube. Cross-sections of air-dried silk tubes demonstrate a more compact structure between the layers which, in turn, creates tubes that tend to be more brittle than their methanol-treated counterparts. The final post-winding processing technique, lyophilization, gives the silk tubes a more porous, lamellar-like structure. Winding structure is typically obscured by the freeze-drying, and the tube surface roughness is increased, as is the tube flexibility. Lyophilized silk tubes have good potential for internal cell seeding as the multitude of interconnected pores should allow significant cell ingrowth. In general post-winding processing is an important component in the generation of tubes with defined properties.

3.3. Porous silk tubes

Porous silk tubes were generated by altering the axial slew rate, with rotational speed held constant, and by changing the number of layers deposited onto the mandrel (Fig. 4). Offsets of 1 mm were introduced to control the spatial distribution of the silk and could be further altered for finer control of tube pore size and distribution. Pore spacing was controlled by the specific winding pattern used, with greater axial slew rates producing pores with greater center-to-center spacing. Using winding pattern B (V_{AXIAL} = 10 mm/s), the pore center-to-center spacing was 1.57 ± 0.06 mm, while using winding pattern C (V_{AXIAL} = 20 mm/s), the

pore center-to-center spacing was 3.73 ± 0.06 mm (Fig. 5b). This pore spacing was consistent over each number of strokes, indicating the fine control of the system. The pore size, however, was controlled by the number of strokes, with increased number of strokes producing tubes with smaller diameter pores. Porous tubes could also be generated by the addition of PEO to the silk, as reported in our previous work[3], or the alternate spinning of PEO and silk itself (not shown), additional methods for generating porous silk tubes.

3.4. Composite silk tubes

Composite tubes were generated by the successive deposition of silk fibroin in multiple winding angles and/or multiple post-winding processing treatment steps (Fig. 5). Fluorescently labeled protein, dextran, or microsperes enabled the visualization of each layer deposited. Two different molecular weight dextrans (2,000,000 MW, tetramethylrhodamine-conjugated; 10,000 MW, Cascade Blue-conjugated) and BSA (66,000 MW, AlexaFluor-488-conjugated) were mixed with the silk solution prior to winding, and minimal leaching between layers was observed after post-winding processing. Composite silk tubes were prepared with up to three independent deposition layers where each layer of silk contained a different molecule of interest (Fig. 5a). Alternatively, fluorescent microspheres (10 μm diameter) in three different colors were used to visualize the windings and layers of silk of a particular tube (Fig. 5b). Finally, composite tubes with different winding patterns and post-winding processing were formed. In Figure 5c, a tube is presented with a lyophilized middle section flanked by two crisscrossed sections on either end, with the entire construct wrapped in a final silk layer. This tube combines the potential for cell-seeding of the porous lyophilized center with the ability to cannulate and suture the tube aided by the patterned, methanol-treated section. The final methanol-treated wrapping of the tube enhances the overall structure and stability of the tube. These composite tubes demonstrate the potential of this approach in forming tubes with spatially defined pores and mechanical properties.

3.5. Mechanical characterization of silk tubes

Mechanical properties of the tubes were assessed using tensile testing to determine the elastic modulus, yield strength, ultimate tensile strength, and elongation to failure. As expected, the methanol-treated and air-dried tubes exhibited the greatest mechanical strength with elastic moduli of 8.35 ± 2.59 MPa and 9.56 ± 0.94 MPa, respectively. Similar trends were seen for the ultimate tensile strength as mean values of 1.12 ± 0.32 MPa for the methanol-treated tubes and 1.74 ± 0.33 MPa for the air-dried tubes were observed (Fig. 6a). These trends suggest that the methanol-treatment and air-drying enhanced the overall protein assembly, β-sheet formation, and shear alignment that provide the mechanical strength of the tubes[18]. The lyophilized tubes, on the other hand, were softer, demonstrating an elastic modulus and ultimate tensile strength of 2.20 ± 0.90 MPa and 0.27 ± 0.11 MPa, respectively. Considering the elongation to failure, values of 46.5 ± 17.1%, 55.5 ± 10.2%, and 27.5 ± 10.9% were recorded for methanol-treated, air-dried, and lyophilized tubes, respectively (Fig. 6a). In comparison with the mechanical properties of the human saphenous vein, the current ‘gold standard’ for arterial bypass grafts, the properties of the silk tubes were on the same order of magnitude as those of the native tissue[29-31] (Fig. 6a). In addition, although not specifically examined in this work, previously fabricated silk tubes using both electrospun and aqueous-dipping methods have demonstrated sufficient radial mechanical properties and burst pressures to maintain the physiological stresses imparted by blood pressure[3, 10]. This overall property matching is critical, as elasticity and compliance mismatch are two of the primary causes of thrombosis in currently available synthetic bypass grafts[32]. However, while the biomechanical properties did nearly match those of a human vein, this system affords more precise control through the use of different winding angles, additional layering, and/or varied post-processing, specifically in the generation of

composite tubes, thus providing a means of dictating biological response *in vitro* and *in vivo* for each specific application.

3.6. Biological evaluation of silk tubes

The biocompatibility of the silk tubes was assessed by step-wise seeding of human smooth muscle cells and endothelial cells *in vitro*. Human coronary artery smooth muscle cells (HCASMCs) and the human umbilical vein endothelial cells (HUVECs) were seeded using a previously described bioreactor system[3], and cultured over a 4-5 day span (3-4 for the HCASMCS, followed by HUVEC seeding). Both cell types attached to the lumen of the tube and were visualized using confocal microscopy (Fig. 6b). This cell attachment suggests the potential to culture functional tissue-engineered vascular grafts *in vitro* prior to *in vivo* implantation. Further control of cell attachment can be controlled through the attachment of cell binding motifs such as RGD-peptides or other functional molecules as described in our previous work[33], and may provide an additional design criteria for tailoring these spun silk tubes for specific tissue engineering applications.

4. Conclusions

Aqueous biopolymer spinning represents a significant advance over current methods for production of tubular constructs, including our previously reported dip methods for production of silk tubular constructs as well as other gel spinning methods used with other degradable polymer systems[15-17]. Furthermore, it differs from currently established artificial silk spinning techniques such as wet spinning[34-37], where fibers are typically drawn into a methanol coagulation bath, and electrospinning[10, 22], where a polymer solution is subjected to a high voltage electric field to generate nanoscale fibers. With the gel spinning approach, fibers are generated from viscous, concentrated silk solutions through the shear forces applied by a small gauge needle. This allows for different winding and post-winding processing options that are not available using the other artificial silk spinning approaches. In addition, gel spinning mimics the natural biochemistry of the silkworm spinneret where issues of fibroin concentration, gelation, and shear are critical parameters for silk spinning[20, 28]. While not presented here, this technique may be combined with the others to further improve tube properties, such as the winding of fibers to improve mechanical strength or with the addition of cells directly into the matrix for more specific biological outcomes. The use of an all aqueous process in this new processing systems allows for the incorporation of labile biological components from growth factors to cells, as we have demonstrated with other modes of silk processing[22, 38]. This establishes unique options for the system to bioengineer tubular scaffolds for a range of biological control, while at the same time exploiting the novel mechanical and biological properties of silk proteins[14], for a variety of applications including microvasculature, intervertebral discs, nerve guides, and other complex composite scaffolds. Altogether, aqueous silk spinning represents a substantial improvement over the prior art with many applications in tissue engineering and beyond.

Acknowledgments

We acknowledge funding from the Tissue Engineering Resource Center (TERC) through the NIH – grant EB002520 from the National Institute of Biomedical Imaging and Bioengineering. We would also like to acknowledge the assistance of Jonathan Kluge in the mechanical testing of the silk tubes and the Tufts machine shop (in particular, Larry McMaster, Scott MacCorkle, and Denis DuPuis) in the construction of the silk winding apparatus.

References

1. Baguneid MS, Seifalian AM, Salacinski HJ, Murray D, Hamilton G, Walker MG. Tissue engineering of blood vessels. Br J Surg. 2006; 93:282–290. [PubMed: 16498591]
2. Kannan RY, Salacinski HJ, Edirisinghe MJ, Hamilton G, Seifalian AM. Polyhedral oligomeric silsequioxane-polyurethane nanocomposite microvessels for an artificial capillary bed. Biomaterials. 2006; 27:4618–4626. [PubMed: 16707157]
3. Lovett M, Cannizzaro C, Daheron L, Messmer B, Vunjak-Novakovic G, Kaplan DL. Silk fibroin microtubes for blood vessel engineering. Biomaterials. 2007; 28:5271–5279. [PubMed: 17727944]
4. Yang Y, Ding F, Wu J, Hu W, Liu W, Liu J, et al. Development and evaluation of silk fibroin-based nerve grafts used for peripheral nerve regeneration. Biomaterials. 2007; 28:5526. [PubMed: 17884161]
5. Jain RK, Au P, Tam J, Duda DG, Fukumura D. Engineering vascularized tissue. Nat Biotechnol. 2005; 23:821–823. [PubMed: 16003365]
6. Fidkowski C, Kaazempur-Mofrad MR, Borenstein J, Vacanti JP, Langer R, Wang Y. Endothelialized microvasculature based on a biodegradable elastomer. Tissue Eng. 2005; 11:302–309. [PubMed: 15738683]
7. Niklason LE, Abbott W, Gao J, Klagges B, Hirschi KK, Ulubayram K, et al. Morphologic and mechanical characteristics of engineered bovine arteries. J Vasc Surg. 2001; 33:628–638. [PubMed: 11241137]
8. Remuzzi A, Mantero S, Colombo M, Morigi M, Binda E, Camozzi D, et al. Vascular smooth muscle cells on hyaluronic acid: culture and mechanical characterization of an engineered vascular construct. Tissue Eng. 2004; 10:699–710. [PubMed: 15265287]
9. Isenberg BC, Williams C, Tranquillo RT. Endothelialization and flow conditioning of fibrin-based media-equivalents. Ann Biomed Eng. 2006; 34:971–985. [PubMed: 16783653]
10. Soffer L, Wang X, Zhang X, Kluge J, Dorfmann L, Kaplan DL, et al. Silk-based electrospun tubular scaffolds for tissue-engineered vascular grafts. Journal of Biomaterials Science, Polymer Edition. 2008; 19:653. [PubMed: 18419943]
11. Sanchez C, Arribart H, Guille MM. Biomimetism and bioinspiration as tools for the design of innovative materials and systems. Nat Mater. 2005; 4:277–288. [PubMed: 15875305]
12. Giraud Guille MM, Mosser G, Helary C, Eglin D. Bone matrix like assemblies of collagen: from liquid crystals to gels and biomimetic materials. Micron. 2005; 36:602–608. [PubMed: 16169238]
13. Moutos FT, Freed LE, Guilak F. A biomimetic three-dimensional woven composite scaffold for functional tissue engineering of cartilage. Nat Mater. 2007; 6:162–167. [PubMed: 17237789]
14. Altman GH, Diaz F, Jakuba C, Calabro T, Horan RL, Chen J, et al. Silk-based biomaterials. Biomaterials. 2003; 24:401–416. [PubMed: 12423595]
15. Kim SH, Kwon JH, Chung MS, Chung E, Jung Y, Kim SH, et al. Fabrication of a new tubular fibrous PLCL scaffold for vascular tissue engineering. J Biomater Sci Polym Ed. 2006; 17:1359–1374. [PubMed: 17260508]
16. Notin L, Viton C, David L, Alcouffe P, Rochas C, Domard A. Morphology and mechanical properties of chitosan fibers obtained by gel-spinning: influence of the dry-jet-stretching step and ageing. Acta Biomater. 2006; 2:387–402. [PubMed: 16765879]
17. Fukae R, Maekawa A, Sangen S. Gel-spinning and drawing of gelatin. Polymer. 2005; 46:11193–11194.
18. Jin, HJ.; Park, J.; Valluzzi, R.; Kim, UJ.; Cebe, P.; Kaplan, D. Bioprocessing of Silk Proteins - Controlling Assembly.. In: Renugopalakrishnan, V.; Lewis, R., editors. Bionanotechnology. Springer; Netherlands: 2006. p. 189-208.
19. Xie F, Zhang H, Shao H, Hu X. Effect of shearing on formation of silk fibers from regenerated Bombyx mori silk fibroin aqueous solution. Int J Biol Macromol. 2006; 38:284–288. [PubMed: 16678253]
20. Asakura T, Umemura K, Nakazawa Y, Hirose H, Higham J, Knight D. Some observations on the structure and function of the spinning apparatus in the silkworm Bombyx mori. Biomacromolecules. 2007; 8:175–181. [PubMed: 17206804]

21. Kim UJ, Park J, Li C, Jin HJ, Valluzzi R, Kaplan DL. Structure and properties of silk hydrogels. Biomacromolecules. 2004; 5:786–792. [PubMed: 15132662]
22. Li C, Vepari C, Jin HJ, Kim HJ, Kaplan DL. Electrospun silk-BMP-2 scaffolds for bone tissue engineering. Biomaterials. 2006; 27:3115–3124. [PubMed: 16458961]
23. Wang X, Kim HJ, Xu P, Matsumoto A, Kaplan DL. Biomaterial coatings by stepwise deposition of silk fibroin. Langmuir. 2005; 21:11335–11341. [PubMed: 16285808]
24. Zhang X, Baughman CB, Kaplan DL. In vitro evaluation of electrospun silk fibroin scaffolds for vascular cell growth. Biomaterials. 2008; 29:2217–2227. [PubMed: 18279952]
25. Nazarov R, Jin HJ, Kaplan DL. Porous 3-D scaffolds from regenerated silk fibroin. Biomacromolecules. 2004; 5:718–726. [PubMed: 15132652]
26. Kim UJ, Park J, Kim HJ, Wada M, Kaplan DL. Three-dimensional aqueous-derived biomaterial scaffolds from silk fibroin. Biomaterials. 2005; 26:2775–2785. [PubMed: 15585282]
27. Wang H, Zhang Y, Shao H, Hu X. A study on the flow stability of regenerated silk fibroin aqueous solution. Int J Biol Macromol. 2005; 36:66–70. [PubMed: 15916801]
28. Jin HJ, Kaplan DL. Mechanism of silk processing in insects and spiders. Nature. 2003; 424:1057–1061. [PubMed: 12944968]
29. Bia Santana D, Armentano RL, Zocalo Y, Perez Campos H, Cabrera Fischer EI, Graf S, et al. Functional properties of fresh and cryopreserved carotid and femoral arteries, and of venous and synthetic grafts: comparison with arteries from normotensive and hypertensive patients. Cell Tissue Bank. 2006; 8:43–57.
30. Han DW, Park YH, Kim JK, Jung TG, Lee KY, Hyon SH, et al. Long-term preservation of human saphenous vein by green tea polyphenol under physiological conditions. Tissue Eng. 2005; 11:1054–1064. [PubMed: 16144441]
31. Donovan DL, Schmidt SP, Townshend SP, Njus GO, Sharp WV. Material and structural characterization of human saphenous vein. J Vasc Surg. 1990; 12:531–537. [PubMed: 2231964]
32. Hoenig MR, Campbell GR, Rolfe BE, Campbell JH. Tissue-engineered blood vessels: alternative to autologous grafts? Arterioscler Thromb Vasc Biol. 2005; 25:1128–1134. [PubMed: 15705929]
33. Sofia S, McCarthy MB, Gronowicz G, Kaplan DL. Functionalized silk-based biomaterials for bone formation. J Biomed Mater Res. 2001; 54:139–148. [PubMed: 11077413]
34. Phillips DM, Drummy LF, Naik RR, De Long HC, Fox DM, Trulove PC, et al. Regenerated silk fiber wet spinning from an ionic liquid solution. J Mater Chem. 2005; 15:4206–4208.
35. Ha SW, Tonelli AE, Hudson SM. Structural studies of Bombyx mori silk fibroin during regeneration from solutions and wet fiber spinning. Biomacromolecules. 2005; 6:1722–1731. [PubMed: 15877399]
36. Trabbic KA, Yager P. Comparative structural characterization of naturally- and synthetically-spun fibers of Bombyx mori fibroin. Macromolecules. 1998; 31:462–471.
37. Liivak O, Blye A, Shah N, Jelinski LW. A microfabricated wet-spinning apparatus to spin fibers of silk proteins. Structure-property correlations. Macromolecules. 1998; 31:2947–2951.
38. Wang X, Hu X, Daley A, Rabotyagova O, Cebe P, Kaplan DL. Nanolayer biomaterial coatings of silk fibroin for controlled release. J Control Release. 2007; 121:190–199. [PubMed: 17628161]

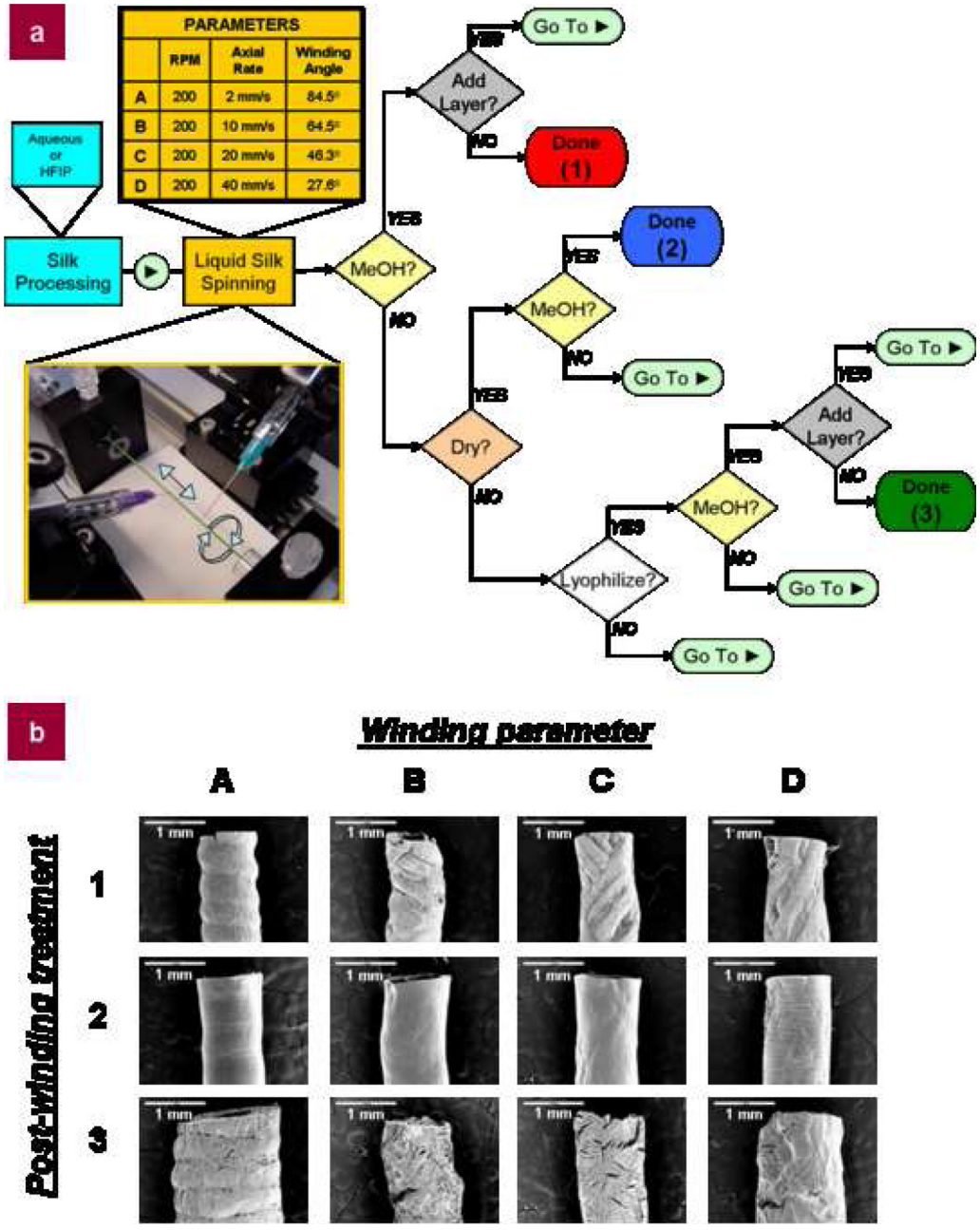

Figure 1. Silk spinning process summary

a, Liquid silk spinning flowchart outlining the tube making process. The process is divided into three main sections: silk processing (aqueous or HFIP), liquid silk spinning (different winding parameters), and post-winding processing. In this study, only aqueous silk processing was used, but the same principles apply to HFIP-derived silk. For winding, four different silk spinning parameters are given, varying axial rate while holding RPM constant (200 RPM). This results in four different winding angles, ranging from a concentric wrapping (axial rate of 2 mm/s) to varied criss-cross patterns (axial rates of 10, 20, or 40 mm/s). For simplicity, these parameters are designated A, B, C, and D, respectively. For post-winding processing, choices include methanol-treatment (1), air-drying (2), and lyophilization (3). Tubes are made by simply following the flowchart. Starting with a

concentrated silk solution, layers may be deposited onto the mandrel using chosen gel spinning parameters (RPM, axial rate). After deposition, the layer may be methanol-treated, air-dried, or lyophilized as part of the post-winding processing. This may complete the tube, but if additional layers are desired, the process returns to the liquid silk spinning process where the same or different winding parameters and post-winding processing conditions may be chosen for subsequent layers until the desired final tube is achieved. Final tubes are named by their chosen winding parameter(s) and post-winding processing (e.g., a tube spun using an axial rate of 2 mm/s and treated with methanol is an 'A1' tube).; **b**, SEM images of example tubes representative of the outcomes achieved through different combinations of winding patterns and post-winding processing treatments (e.g., the tube at the top left is a tube made using winding parameter A (200 RPM, axial rate of 2 mm/s) and post-winding treatment 1 (methanol)).

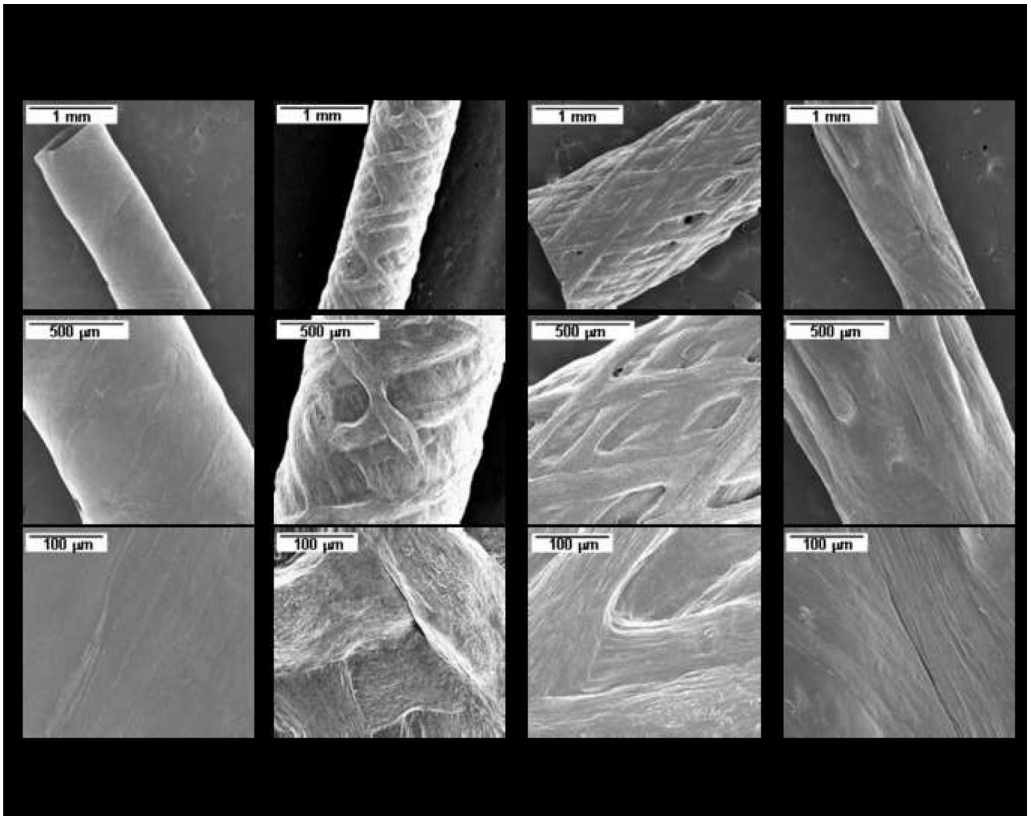

Figure 2. Silk spinning winding patterns

Silk tubes generated using different winding patterns with the same post-winding processing treatment (1, methanol-treated). Axial rate increases from left to right from 2 mm/s (A1) to 40 mm/s (D1). Different magnifications are given to demonstrate the complexity and control of the winding process.

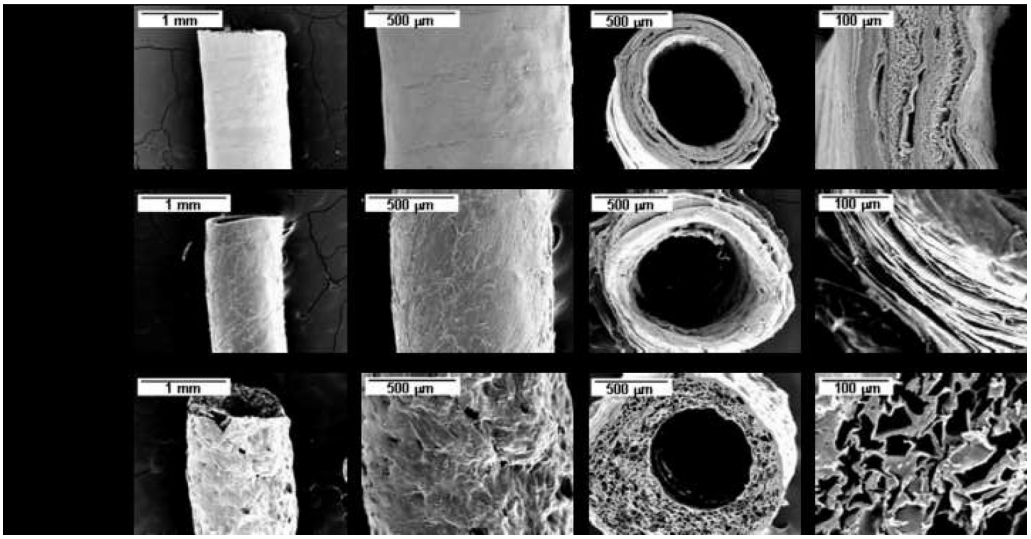

Figure 3. Silk spinning and post-winding processing

Silk tubes generated using the same winding pattern (A, V_{AXIAL} = 2 mm/s) with different post-winding processing. From top to bottom, tubes are methanol-treated (A1), air-dried (A2), and lyophilized (A3). Longitudinal (columns 1 and 2) and cross-sectional views (columns 3 and 4) are given to demonstrate the differences in tubes made using the different post-winding processing techniques.

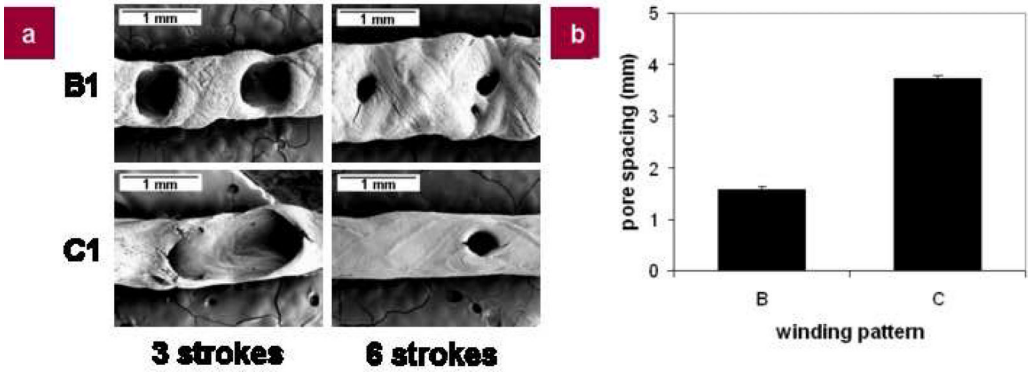

Figure 4. Control of silk tube pore size and distribution

a, SEM images of porous silk tubes generated using different winding patterns (B and C, V_{AXIAL} = 10 and 20 mm/s, respectively) and different numbers of strokes (3 or 6 strokes). All tubes were treated with methanol for post processing; **b**, Plot of center-to-center pore spacing based on the different winding patterns. Center-to-center pore spacing was consistent over all numbers of strokes.

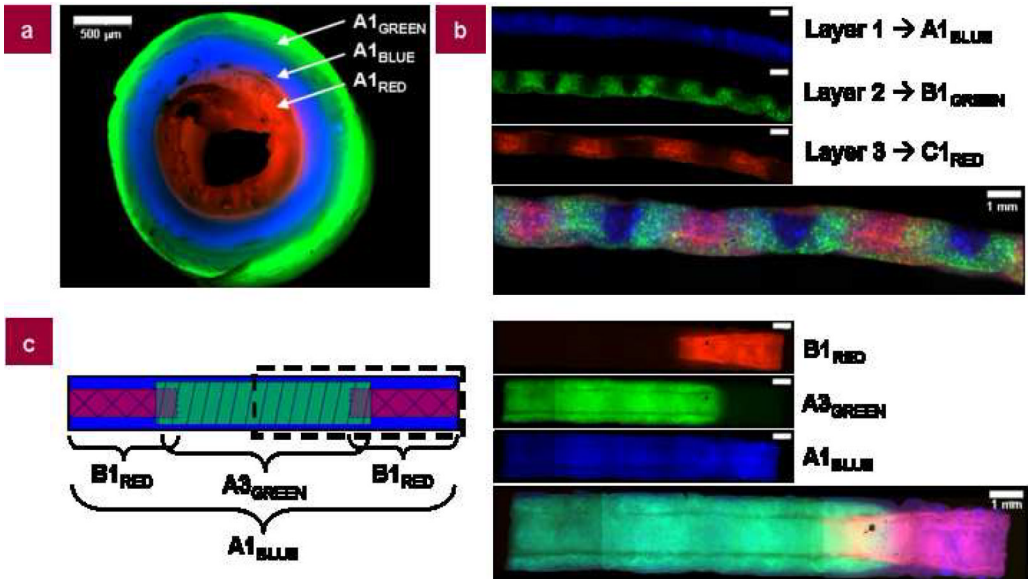

Figure 5. Composite silk tubes

Silk tubes generated with different silk compositions, windings, and post-winding processing steps. **a**, Silk tube generated using silk mixed with either dextran or BSA where the inner layer is silk mixed with tetramethylrhodamine-conjugated dextran (2,000,000 MW), the middle layer is silk mixed with Cascade Blue-conjugated dextran (10,000 MW), and the outer layer is silk mixed with AlexaFluor-488-conjugated BSA (66,000 MW). Each layer was spun using the same winding pattern (A, V_{AXIAL} = 2 mm/s) with the same post-winding processing treatment (1, methanol-treated); **b**, Silk tube generated using silk mixed with different color fluorescent polystyrene microspheres (10 μm diameter; red, blue, and green). Each layer was spun using a different winding pattern where the inner layer was silk with blue microspheres spun using winding pattern A (V_{AXIAL} = 2 mm/s), the middle layer was silk with green microspheres spun using winding pattern B (V_{AXIAL} = 10 mm/s), and the outer layer was silk with red microspheres spun using winding pattern C (V_{AXIAL} = 20 mm/s). The composite silk tube is shown below the images of individual layers; **c**, Composite silk tube generated according the diagram where the ends of the tube are the silk mixed with tetramethylrhodamine-conjugated dextran, wound using winding pattern B, and methanol-treated (treatment #1); the middle of the tube is the silk mixed with AlexaFluor-488-conjugated BSA, wound using winding pattern A, and lyophilized (treatment #3); and the entire tube is wrapped using the silk mixed with Cascade Blue-conjugated dextran, wound using winding pattern A, and methanol-treated (treatment #1). The schematic diagram of the tube is given on the left and the section outlined by the dotted lines is imaged on the right with each individual color/layer and the composite tube below.

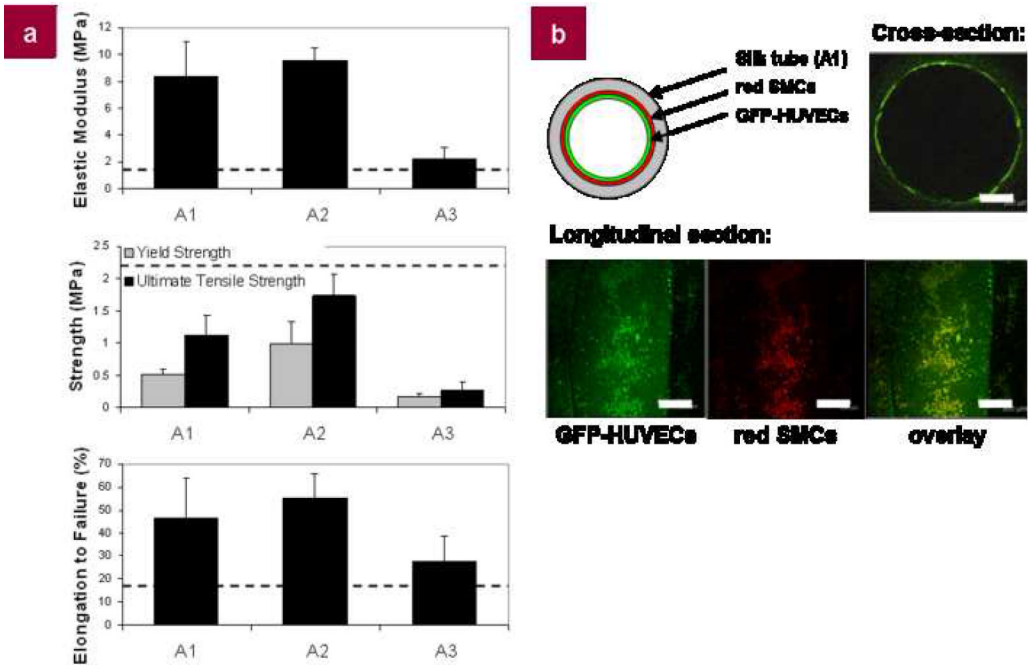

Figure 6. Biological and mechanical evaluation of silk tubes

Silk tubes were generated with different post-winding processing and evaluated for mechanical strength as well as for cell attachment and ingrowth with different cells types (HUVECs and SMCs). **a**, Evaluation of elastic modulus, yield strength, ultimate tensile strength, and elongation to failure of silk tubes. Tensile tests were performed hydrated in PBS in a temperature-controlled bath (37.0 ± 0.3°C). Dotted lines represent the previously-reported elastic modulus[29], ultimate tensile strength[30], and elongation to failure[31] of a human saphenous vein; **b**, Diagram and fluorescent images of a cell-seeded silk tube. HUVECs are transduced with GFP and SMCs are dyed using a red fluorescent cell tracker dye. Cross- and longitudinal sections of the tube are given. All scale bars are 300 μm.